



# Aerial Robot for Sewer Inspection



PDTI Urban Challenge

## D2.2 Towards automatic sewer inspection. First results

Grant Agreement Number	601116 (corresponding to ECHORD Plus Plus Project)
Call identifier	FP7-ICT-2011-9
Project Acronym	ARSI
Project Title	Aerial Robot for Sewer Inspection
Funding Scheme	CP - Collaborative project (FP7)
Project Starting date	01/01/2016
Project Duration	34 months (including 4 months of evaluation periods: M7-M8 and M21-M22)
Deliverable Number	D 2.2
Deliverable Title	ARSI phase 1 test results
Nature of Deliverable	R
Dissemination Level	RE
Due date of deliverable	M6
Actual Date of deliverable	30/06/2016
Produced by	FCC (Albert Figueras, Raúl Hernández, Tamara Pintado) EURECAT (François Chataigner, Pedro Cavestany, Sergi Caselles, Daniel Serrano) SIMTECH (Marcel Corominas, Aleix Cortada) IBAK (Manfred Weber)
Reviewed by	FCC (Albert Figueras, Xavier Grau) EURECAT (Daniel Serrano, Jesús Pablo González)
Validated by	FCC (Albert Figueras, Xavier Grau)



*This project has received funding from the European Union's Horizon 2020 Research and Innovation Programme under Grant Agreement no. 601116*

## Reference Documents

Issue Date	Version	Title
29/12/2014	N/A	ECHORD++ PDTI Urban Robotics – Challenge Brief – “Utility Infrastructures and condition monitoring for sewer network. Robots for the inspection and the clearance of the sewer network in cities”.
14/03/2015	v1.0	Aerial Robots for Sewer Inspection (ARSI) Consortium Proposal Document
07/06/2016	N/A	ECHORD++ PDTI Urban Robotics – Evaluation Criteria Phase I
30/06/2016	v1.0	D2.1 ARSI operation requirements and system design

## Document change record

Issue Date	Version	Title
30/06/2016	V1.0	Release of the document

Acronyms and definitions	
ARSI	Aerial Robot for Sewer Inspection
ESC	Electronic Speed Controllers
MAV	Micro Aerial Vehicle
MEMS	Micro-Electro-Mechanical Systems
MEMS	Mean Time Between Failures
MTOW	Maximum Take-Off Weight
PDTI	Public end-user Driven Technological Innovation
ROS	Robotic Operating System
RPM	Revolutions Per Minute
UAV	Unmanned Aerial Vehicle

## Table of Contents

1	Introduction.....	9
1.1	Objective and scope .....	9
1.2	Structure of the document.....	9
1.3	Summary of field tests.....	9
2	Robotic platform .....	11
2.1	Test plan .....	11
2.2	Preliminary flight tests.....	11
2.2.1	Objectives .....	11
2.2.2	Results .....	12
2.2.3	Lessons learned .....	12
2.3	May 19 <sup>th</sup> – Initial tests of ARSI prototype on the sewer .....	12
2.3.1	Objectives.....	12
2.3.2	Results .....	13
2.3.3	Lessons learned .....	13
2.4	June 3 <sup>rd</sup> – Confined space flights with the first prototype.....	14
2.4.1	Objectives.....	14
2.4.2	Results .....	14
2.4.3	Lessons learned .....	14
2.5	Validations of the final prototype in Eurecat .....	15
2.6	June 23 <sup>rd</sup> – validation flight tests with reduced payload .....	17
2.6.1	Objectives.....	17
2.6.2	Results .....	17
2.6.3	Lessons learned .....	18
2.7	June 30 <sup>th</sup> – final flight tests .....	18
2.7.1	Objectives.....	18
2.7.2	Results .....	18
2.7.3	Lessons learned .....	20
3	Cameras and illumination .....	21
3.1	Choice of cameras and lenses .....	21
3.1.1	Cameras.....	21
3.1.2	Lenses .....	21
3.2	Choice of LEDs .....	21

3.3	Development of camera drivers .....	22
3.4	Experiments and results .....	22
3.4.1	<i>Preliminary test - 2016/01/29</i> .....	22
3.4.2	<i>Second test - 2016/03/10</i> .....	24
3.4.3	<i>Third test - 2016/05/19</i> .....	24
3.4.4	<i>Fourth test - 2016/06/09</i> .....	24
3.4.5	<i>Further design</i> .....	24
4	Communications .....	25
4.1	Test area .....	25
4.2	Wireless propagation simulations in sewers:.....	26
4.2.1	Wireless propagation measuring campaign.....	27
4.2.2	Wireless network full coverage test.....	29
4.3	Bandwidth measurement results .....	29
4.4	Antenna polarization .....	31
4.5	Video-streaming .....	31
5	Autonomous flight modes.....	32
5.1	Software design and implementation .....	32
5.2	Test setup .....	33
5.2.1	Simulator .....	33
5.2.2	Remote control.....	34
5.3	Test results.....	34
6	Remote station.....	36
6.1	Integration with Dracma .....	36
6.2	Remote station plugins.....	36
7	Annex A: References .....	38

## Figure list

Figure 1: Quadrotor flight in Passeig Sant Joan in Barcelona .....	12
Figure 2.- Validation of the adapted landing gear for specific sewer sections.....	14
Figure 3: Flight tests at the Eurecat indoor flying arena.....	16
Figure 4 Flight test log of the ARSI platform with the final configuration.....	17
Figure 5 Photos of the flight tests on June 30 <sup>th</sup> .....	19
Figure 6 ARSI platform during a realistic inspection operation on the June 30 <sup>th</sup> .....	20
Figure 7 Example of the data collection prototype (left) and the operational area (right).....	23
Figure 8 Image taken by the camera in the front of the platform (left) and its rectification (right).....	23
Figure 9 Image taken by the camera on the side of the platform (left) and its rectification (right) .....	23
Figure 10 Test area near Passeig Sant Joan in Barcelona .....	25
Figure 11 Example of sections and turns .....	25
Figure 12 Simulation of wireless propagation in the sewer, using the real cross-section .....	26
Figure 13 Travelled path in communication along Valencia .....	27
Figure 14 Measured received signal power along Valencia.....	27
Figure 15 Traveled path in communication along Bailén and Mallorca .....	28
Figure 16 Measured received signal power along Bailén and Mallorca .....	28
Figure 17 Network deployment to provide coverage along Valencia, Bailén and Mallorca ..	29
Figure 18: Bandwidth link test example using JPERF .....	30
Figure 19: Bandwidth link test results.....	30
Figure 20: High-level design for the ARSI flight modes.....	32
Figure 21: Tunnel mode simulation in RVIZ. Wall detections (in red) are extracted from simulated laser data (in white) to produce tunnel estimations (in blue) used to calculate control requests allowing the vehicle to autonomously follow the tunnel.....	33
Figure 22: Our tunnel Follow flight mode keeps the vehicle at the centre of the tunnel without human interaction.....	34
Figure 23: ARSI Wi-Fi coverage displayed in Dracma.....	36
Figure 24: ARSI Remote Station .....	37

## Table list

Table 1. List of field tests.....	10
Table 2 Specifications of the two selected lenses with respect to the requirements of the camera.....	21
Table 3: Simulation and Experimental propagation results.....	28

This page is intentionally left in blank

## 1 Introduction

### 1.1 Objective and scope

This document corresponds to the deliverable “D2.2 Towards automatic sewer inspection. First results” of the ARSI consortium, covering the preliminary results of phase I System Design of the Urban Robotics Public end-user Driven Technological Innovation (PDTI) of the ECHORD++ project. Details about system design, logistics and economic viability are provided in deliverable D2.1.

The aim of this deliverable is to report the initial outcomes of our experiments. A set of tests have been conceived to validate the main design principles described in D2.1 and, thus, demonstrate the technical feasibility of the concept. These tests have been organized around the key challenges and risks identified during the design.

### 1.2 Structure of the document

The document is organized as follows:

- Section 1: (current section) introduces the objectives and scope of this deliverable
- Sections 2 to 6 report on the preliminary results for each test:
  - Aerial platform configuration
  - Cameras setup and illumination
  - Communications
  - Flight modes
  - Remote station and integration with sewer inspection systems
- Section 7: concludes the document with the key remarks and way forwards

### 1.3 Summary of field tests

The ARSI consortium has organized a comprehensive test campaign to validate the initial developments of the project. The following sections provide details about them.

In general terms, there have been three different levels of tests: simulation, in-lab and field tests. Simulation tests were particularly suited for the validation of software concepts and prototyping algorithms. Most of the platform and flight tests in this initial phase were in-lab tests. These were carried out on Eurecat premises, using an indoor flying area equipped with a motion tracking system, to ensure a safe and controlled environment for initial validations of new configurations.

Finally around 10 field tests were carried out onsite in the sewers of Barcelona, in two different locations: Passeig Sant Joan and Avenida Pedralbes. Field tests were typically organized around specific objectives, for instance: validating platform controllability with full payload in the sewer; identifying signal behaviour; validating the ARSI Concept of Operation from the communication perspective, or from the operational perspective.

The following table summarizes the series of field tests done on sewer conditions:

Table 1. List of field tests

<i>Date</i>	<i>Location</i>	<i>Objectives</i>
2016/01/20	Passeig Sant Joan-Valencia	Initial data collection for the prototyping of the payload.
2016/29/01	Av. Pedralbes	Data collection in extreme sewer sections. Initial testing of visual system
2016/02/17	Passeig Sant Joan-Valencia-Bailén	KoM: Visit to sewers. Analyse visual and structural condition.
2016/03/10	Passeig Sant Joan	First flight tests with a small multirotor. New camera model and LEDs configuration tested.
2016/04/15	Passeig Sant Joan-Valencia-Bailén-Mallorca	Communication tests. Characterize wireless propagation: attenuation, path loss, periodic fadings. Wireless network design and test.
2016/05/19	Passeig Sant Joan	First flight tests of ARSI prototype (platform+payload). Analyse turbulence, stability and conditions in Passeig Sant Joan. Autonomy and illumination tests.
2016/06/03	Passeig Sant Joan-Valencia	Second flight test: Validation of Pixhawk controller. Platform empty. Incident with a motor.
2016/06/09	Passeig Sant Joan-Valencia-Bailén-Mallorca	<ul style="list-style-type: none"> <li>• Communication tests. Bandwidth measurements of the link between the robot and the base station.</li> <li>• Lightning condition test: try different illumination setups.</li> <li>• Video streaming tests.</li> </ul>
2016/06/23	Passeig Sant Joan-Valencia	Third flight test. Analyse turbulence, stability and conditions in Valencia. Platform with reduced payload. Feasibility demonstrated.
2016/06/30	Passeig Sant Joan-Valencia	Fourth flight test. Final system with full payload weight.

## 2 Robotic platform

### 2.1 Test plan

In this section we describe the various tests carried out with the ARSI aerial platform following the design deliverable D2.1. The platform was tested extensively, both in the indoor flying arena at Eurecat (Figure 3) and in real sewer environments at Passeig Sant Joan in Barcelona (Figure 1).

For this project, the flying conditions in the sewers were also recreated in a narrow corridor in Eurecat. The corridor altitude and shape was slightly different from that of a typical sewer tunnel, but it still provided us with a very useful controlled environment for an initial validation of the dynamics of each platform configuration.

Our standard testing procedure is designed to ensure system reliability. Each configuration was tested in a series of experiments of incremental complexity. Typically:

- Lab test of each subsystem: motors, speed controllers, power distributors, illumination, etc.
- Indoor flight test campaign:
  - Basic flight of the empty platform (no payload) to validate electronics and autopilot
  - Stress tests: each new configuration goes through a set of intensive flights to validate the reliability of the platform.
  - Autonomy test: the real autonomy in nominal conditions is assessed.
  - Functional test: specific to each test, a particular aspect of the functionality is tested.
- Field tests: the same series of incremental tests are performed in realistic conditions.

Despite the deep background and experience held within the ARSI consortium, both in the design and operation of aerial platforms and work in sewer environments, we were very aware of the complexity of this project and expected that many of our assumptions in terms of platform design and operation would be proved wrong during these test campaigns.

Therefore we approached these validation tests as an iterative process, where results and issues were analysed, to learn lessons resulting both in modifications to our design and changes in the selection of platform components. This parallel and collaborative development process was very successful and positive, allowing us to converge rapidly towards a functional prototype and a robust system design for the next phases of this project.

The following sections describe the evolution of the robotic platform.

### 2.2 Preliminary flight tests

#### 2.2.1 Objectives

The goal of these tests was to gather hands-on experience early on in the project, and a better understanding of the challenges of flying multirotor vehicles inside sewer tunnels, in particular in terms of dynamics, turbulences and control.

## 2.2.2 Results

A flight with a small commercial multirotor (Figure 1) without payload was used as proof of concept to show the basic feasibility of the concept.



Figure 1: Quadrotor flight in Passeig Sant Joan in Barcelona

## 2.2.3 Lessons learned

The objective was for team members to appreciate the complexity of operations in the sewer environment. Interactions with sewer inspection staff served to elicit their operational needs, and direct the conceptualization of the solution towards their expectations. This helped the ARSI partners to gain insight into the practicalities of sewer inspection, and triggered the conceptual design of the ARSI vehicle.

This test also helped to better understanding the logistics and operational procedures for sewer inspections. Basic design principles of ARSI such as the enhanced flight modes, the selection and location of sensors, the integration with current inspection protocols, etc. were strongly inspired by this test.

In terms of objective for the phase 1 of ARSI, and within the context of the PDTI Urban Challenge project brief, the consortium agreed to prioritize developments in line with the expected demonstration in the evaluation of the first results (mobility, autonomy and communications). This implied focusing on prototyping the aerial platform rather than the onboard software. Due to the limited amount of time and resources for phase 1, the consortium agreed that the platform would be tele-operated for the evaluation, without any onboard autonomy. We also agreed to prioritize communications tests and the development of a feasible Concept of Operation, since the aerial platform differs in many aspects from other type of robots. However, we also attempted to partially implement some of the onboard and operator software, including the specialized flight modes, onboard control algorithms (section 5) and ARSI Remote Station (section 6), in order to demonstrate some their future functionality.

All these decisions clearly influenced the results described in this document.

## 2.3 May 19<sup>th</sup> – Initial tests of ARSI prototype on the sewer

### 2.3.1 Objectives

An initial prototype was developed by the ARSI consortium. This system corresponds to the first configuration shown in the Propulsion chain analysis in D2.1. Even though not optimal, the components were mostly available among the partners and an initial validation of the entire system, including sensors, was worth doing at earlier stages of the project.

The goal of these tests was to carry initial flights in the sewers using the final configuration in terms of weight. The specific objectives were:

- Allow SimTech pilots to practice flight inside the sewers;
- Validate the theoretical analysis of expected flight times
- Compare current configuration against the Autonomy test of the ECHORD++ evaluation process;
- Evaluate any differences in behaviour or control with previous test flights at Eurecat.

### 2.3.2 Results

A first flight was carried out in the Passeig Sant Joan section of the sewers, which is much larger (~2m) than standard sections and therefore much easier to fly in. The vehicle was landed at the end of the tunnel, then flown again to return and land at its start position, all with a single battery charge. The flight was successful and met the Autonomy criteria defined by for the ARSI PDTI.

A second flight was carried out in the Valencia section of the sewers which, with a width of ~1m is much narrower than Passeig Sant Joan and therefore much more challenging for pilots. Our pilot was able to fly ~30m of the ~70m required to meet the evaluation criteria, but clearly piloting in such conditions was very challenging, and the platform came in contact several times with the tunnel walls, causing two propeller protectors to part. At this point we decided that it was safer to abort the flight to avoid damaging the platform or its sensors, and to focus instead on how we could learn from this test to facilitate future flights.

It is important to note that while the final ARSI system will offer semi-autonomous flight modes allowing easy navigation in narrow tunnels, the system at this stage (Phase I) only allows for manual control by a pilot. The task of flying in a narrow tunnel like Valencia is therefore much more complex for pilots now than it will be during Phase II of the project.

### 2.3.3 Lessons learned

The first lesson learned in these first tests was that the 3D-printed shields mounted on the rotors were too fragile to effectively protect the propellers. **More robust propeller shields** would need to be developed.

It was also clear that flying in such narrow spaces in full manual mode was extremely challenging and that using the **more advanced flight modes** offered by the Pixhawk (attitude or altitude control) would be extremely advantageous.

This test also triggered some other improvements on the platform such as adaptations required to the landing gear to facilitate landing on uneven ground, better location of illumination, etc. Most importantly, the test helped gather experience of real inspections operations with the ARSI platform. The following images shows the final design of the landing gear to allow landing on buckets with narrow curb:



Figure 2: Validation of the adapted landing gear for specific sewer sections

## 2.4 June 3rd – Confined space flights with the first prototype

### 2.4.1 Objectives

The goal of these tests was to follow up on the initial flights and evaluate the various modifications made to the platform. In particular, the objective was to use the Pixhawk Altitude Control mode, which uses the atmospheric pressure sensor to stabilize the platform vertically without any input from the pilot. For these tests, a platform configuration using 2 LIPO batteries was used, in order to increase flight time and facilitate the pilot's task.

### 2.4.2 Results

An initial flight was carried out successfully in the wide tunnel of Passeig Sant Joan where the Altitude Control mode was tested successfully.

A second flight was carried out in the Valencia tunnel; unfortunately it resulted in a crash after a few seconds, seemingly due to a fault in the front-right rotor of the platform. Several parts of the platform were damaged, including shields, propellers and landing gear.

### 2.4.3 Lessons learned

An investigation was carried out to determine the reasons for the crash. Based on the analysis of various mission logs (motor RPMs, power consumption, etc.), we established that the incident was not caused by any malfunction in the control systems; therefore, it was determined that the likely reason was electrical or mechanical.

A low battery alarm was triggered a few seconds before the unfortunate event, which shows a drastically reduced flight time for this specific setup. A-posteriori analysis showed that the use of the second battery increased the total weight of the platform so much that its performance was pushed close to its theoretical limits. This is shown in the second configuration of the Propulsion chain analysis in D2.1. The consortium determined that the strong turbulences caused by the increased weight, and therefore, increased airflow, brought the drive components (speed controller and motor) to a strain that eventually caused a malfunction in the motor. The team also performed an intensive post-accident analysis and

test for each component, and was able to sporadically recreate the failure on this specific motor.

This test triggered a deep re-design of the platform prototype for phase 1. In particular, higher quality motors and propellers were installed despite the budget limitations in this initial phase, to increase reliability and Mean Time Between Failures (MTBF). Note that despite the slight increase in component costs, this does not affect the economic viability of the solution as described in deliverable D2.1. It is also worth mentioning that component failures are normal after prolonged use in aerial robotics systems, as was the case for some of the parts as they were recycled from previous projects by the partners to limit costs. It is therefore essential that maintenance protocols are respected to keep track of operational time at component level, and to replace these components when their lifetime is approaching its end. The issue identified in this test was likely caused by both the use of low-end components for the first version of the prototype, and the stress caused by pushing the limits in terms of weight as part of the iterative design of our project.

The redesign is the final configuration described in D2.1. Furthermore, as lessons learned, we decided not to aim at maximizing performance by pushing the physical limits of the system in this phase; and to prioritize reliability and robustness instead, keeping the platform within reasonable margins and allowing for contingency in the selection of the components. Even though the current documents describe what we think it is the optimal design, during the lifetime of the project these two principles will remain as key principles for any possible improvement or optimization.

## 2.5 Validations of the final prototype in Eurecat

The final components selected and described in deliverable D2.1 were thoroughly tested in Eurecat indoor flying area (see Figure 3). Several flight tests were performed in Eurecat in order to confirm the theoretical analysis made for motor and battery design detailed in D2.1. The objectives were to accurately evaluate both platform autonomy and control stability in different configurations, both nominal (open spaces) and confined or narrow spaces.



**Figure 3: Flight tests at the Eurecat indoor flying arena**

The final configuration of the platform used during these tests is:

- Custom-made TBS discovery frame
- Motors: 4 x T-Motor MN3110 780KV
- Propellers: 4 x carbon fiber T 10x3.3"
- ESC: 4 x ESC 30A
- Batteries: 1 x GensAce 6000mAh 4S 35C
- Payload: 600g

For this configuration, the results of the analysis in terms of flight time and throttle were the following:

- Flight time: 9.9min
- Throttle: 71%

This shows an error of approximately 1.5% when comparing the theoretical analysis described in D2.1 with experimental results. This coincides with previous tests and validates also capacity of the team to design any future adaptation or optimization to the system if the requirements change.

The following figure shows a log of one of the flights made in Eurecat. However, in this flight we have pushed the limits of the batteries showing up to 12 minutes. This would be not advisable in nominal circumstances but shows the margin in case of emergency:

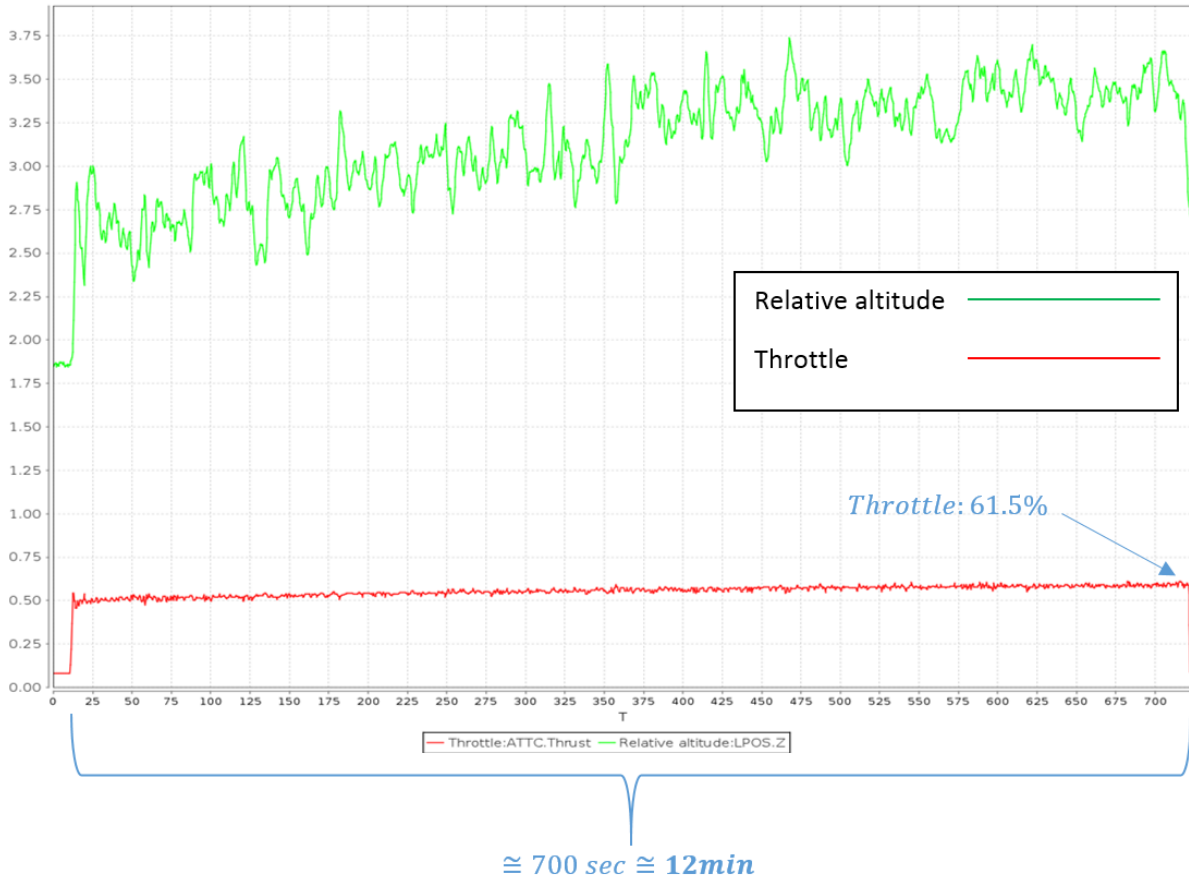


Figure 4 Flight test log of the ARSI platform with the final configuration

The ARSI consortium carried another 2 sets of field tests in the Barcelona sewers to validate this configuration, which are detailed in the following sections.

## 2.6 June 23rd - validation flight tests with reduced payload

### 2.6.1 Objectives

Following the previous flight tests, the team decided to revert to a 1-battery configuration, using more powerful motors as well as more rigid carbon fibre propellers. Flight tests with this configuration in the Eurecat flying arena showed that a lighter platform provided more stable control, despite a slight drop in vehicle autonomy.

Given the complexity for pilots to fly in narrow sewer tunnels with little illumination, we decided that priority should be given to stability and safe flight in this early phase of the project; and that other battery configurations would be evaluated after the ARSI tunnel-specific flight modes have been developed.

### 2.6.2 Results

Unfortunately, due to limited stock on our suppliers, the carbon fibre propellers did not arrive on time for this test. Therefore, according to the analysis described in D2.1, we reduced the weight of the payload to stay within safety limits. The configuration for this test included the final motors and electronic components, but the APC SF propeller from previous tests.

Intensive flights were performed to ensure the reliability and robustness of the electrical side of the system. Both manual and altitude control were tested. Following these tests, the redesign of the system was approved, with the exception of the propeller model to be used.

### 2.6.3 Lessons learned

During this test, the platform behaviour was stable and smooth showing that the need to carry more sensors for inspections pushes the complexity of the control. This also confirms the need for onboard autonomous algorithms to help pilot during inspections, as described in deliverable D2.1.

## 2.7 June 30th – final flight tests

### 2.7.1 Objectives

The objective for this tests was to validate and prepare the platform and the team for the evaluation of the ECHORD++ PDTI.

### 2.7.2 Results

On the last test before the evaluation, the final setup was used, including full payload weight and carbon fibre propeller. As for previous tests, and according to the design decisions described in D2.1, only one battery was used.

After the replacement of the propeller, the platform control was fine-tuned at Eurecat. The stability of this system increased drastically compared to the previous test, even with the full payload weight. This is partially due to the use of better quality carbon fibre propellers, confirming the selection of components described in D2.1.





Figure 5 Photos of the flight tests on June 30<sup>th</sup>

The results of the rehearsal of the ECHORD++ Urban Challenge PDTI evaluation are summarized in this table (see section 0 for Communication test):

<b>Mobility Test</b>	
100 m straight line	ARSI pilot could fly manually and stable at different speeds and altitudes. At a nominal inspection speed, the ARSI solution could inspect the segment in Passeig Sant Joan in around 100 sec at a nominal speed of 1m/s. Some other tests evaluated the stability of the platform at lower speeds (0.5 m/s) and at full speed without compromising the mobility.
100 m with 90° curve	This test implies the flight in C\Valencia with a much narrower section. This obviously reduced the maximum flight time that a pilot can use when flying manually without support from specific flight modes for sewer inspection that will be developed in future phases. ARSI pilot could fly several times at constant speed and altitude, starting from Psg. Sant Joan, traversing along the straight line, turning a 90° curve and flying at nominal inspection speed all 100 m (longer than in the evaluation) until the end of this segment in the intersection with C\Bailen.
Recovery test	After the modifications to the landing gear, several tests were carried out to take off from the bucket in different inclinations. This has not shown any problems in our experiments.
<b>Autonomy Test</b>	
Demonstrate that in 8 hours we can arrive to 1Km	According to our experiments, the platform autonomy (maximum flight time) depends on the inspection speed. For a nominal speed of 0.5 m/s, the platform is able to inspect 300m on a single battery, with an equivalent flight time of 10 minutes. Therefore, a forecast of the maximum theoretical distance inspected in 8 hours would be 1.8km/h or 14.4km/8hours. This is a direct extrapolation of the platform performance in a <b>theoretical</b> case. For the

	<b>realistic</b> analysis, including all operational and logistics constraints, please refer to the appropriate section in D2.1.
--	--

According to the results of these tests, the consortium considers that the feasibility of the solution has been demonstrated, the medium level risks identified at the beginning of the project have all been evaluated or even removed as described in D2.1.

The consortium is aware of the technological challenges, but is confident that they will be met by our comprehensive design and work plan. ARSI prototype is ready for the evaluation.



Figure 6 ARSI platform during a realistic inspection operation on the June 30<sup>th</sup>

### 2.7.3 Lessons learned

At this stage of the development, the operation still requires of a skilled pilot, but this limitation will be overcome during next phases of development.

### 3 Cameras and illumination

This section describes the criteria of design and first results obtained in the experiments made on the vision system of the platform.

#### 3.1 Choice of cameras and lenses

##### 3.1.1 Cameras

The constraints on size and weight imposed by the platform has led us to the selection of the [UI-3251LE-M-GL](#) ueye camera. This board camera is light (12 gr), small (less than 9 cm<sup>2</sup>) and offers a wide set of features and capabilities that the challenging conditions of the sewer make necessary in order to obtain reliable imagery for post-processing. These traits are its resolution (2MP), high rate (up to 60 Hz), and a set of settings which allow to adapt the images to the lack of light typical of the working environment (pixel clock, exposure, gain, black level, gamma, etc)

##### 3.1.2 Lenses

The specific nature of this project (aerial platform) and the requirements that the defect inspection system should meet (coverage of the whole section of the sewer: walls, floor and ceiling) make mandatory the use of fish-eye lenses. We have narrowed down the selection of the lenses to two models: [BFM1220C](#) and [BF2M15520C](#). Both lenses are fish-eye (Angle of View larger than 180°). The specifications of both lenses along with the requirements of the camera are shown in this table:

**Table 2 Specifications of the two selected lenses with respect to the requirements of the camera**

Model	Resolution	Image sensor size	weight
BFM1220C	1,4MP	1/3"	6gr
BF2M15520C	2MP	1/2"	21gr
Camera UI-3251	2MP	1/1,8"	-

It is clear that the lens BF2M15520C adjusts better to the camera UI3251, but its weight penalises it (there will be 4 cameras mounted, see D2.1). We therefore will keep both models until we figure out whether is more critical to the design the quality of the imagery or the limitations on weight.

#### 3.2 Choice of LEDs

Multiple options and LEDs settings have been tried before reaching the optimal configuration for our system. As explained in D2.1 we use CREE LEDs for lighting the scene covered by the front and rear cameras and VOLO LEDS for the sides. The intensity consumed by the LEDS has been experimentally adjusted in several tests in situ to match lighting needs and power consumption rate. In these experiments the position of the LEDS with respect to the cameras and their number have also been iterated (see D2.1 for final design)

### 3.3 Development of camera drivers

Starting from a driver for a [general ueye camera developed by the ROS community](#), we have developed a specific driver with much more control over the settings of the cameras, so that we can tailor them for the working conditions of the sewer and integrate the driver with our ROS system. Apart from tinkering with the image configuration system, our driver allows us to take images with a certain exposure time and frame ratio (typically 30 Hz) but store in disk images in a different frame ratio (typically 10 Hz) so that images are focused and blurring is avoided (highly probable artefact due to the proximity of the walls to the platform) while keeping down the use of CPU and disk memory.

Alongside the development of the driver of the cameras we have implemented two rectification methods in order to undistort the images provided by the fish-eye lenses (one based on OpenCV and other based in [Scaramuzza calibration tool](#)). Although the results obtained are satisfactory, we will keep investigating other methods to optimise the undistortion and CPU consumption.

As explained in D2.1 the data streamed by the cameras is taken by our ROS nodes and stored in rosbag files.

### 3.4 Experiments and results

The performance of the cameras, as well as the behaviour of the lenses and light cast by the LEDs have been tested jointly in the experiments. The evolution of the design with the experiments conducted is explained here succinctly.

#### 3.4.1 Preliminary test - 2016/01/29

The initial choice for the camera was the [PointGrey Firefly MV 1394a](#), along with the lens BFM1220C and 4 VOLO LEDs. Another lens of AOV 70°, BW38BLF, was also considered. Stereo cameras were discarded due to weight and CPU consumption.

In this experiment the variables resolution, frame rate, gain and exposition time were found to be crucial as well, in order to avoid blurred images, low definition and too dark scenes. Furthermore, the continuous movement of the platform pronounces the blurring effect. These observations led us to purchase the ueye camera which ensures that the image requirements for sewer inspection are met.

Lighting conditions are critical in order to obtain images of quality enough to be post-processed. The VOLO LEDs were validated, although we decided to add more units (4 VOLO LEDs per camera) and distribute them along the platform so the light cast by them was less direct.

The fish-eye lens proved to be necessary. Given weight and CPU constraints, it was decided to use 4 cameras on the platform (see D2.1). If the visual system was to cover the whole section with 4 cameras, fish-eye were indispensable. Therefore the lens BW38BLF was taken out of the design.

The following images shows the sensor payload prototype developed only for the purpose of data collection. They correspond to same tests in the sewers in Av. Pedralbes (Barcelona), a much narrower and non-illuminated section of Barcelona sewer network:



Figure 7 Example of the data collection prototype (left) and the operational area (right)

Figure 8 and Figure 9 show images taken in the first experiment, along with the rectification performed by our software. It can be noticed that the light cast by the LEDs focuses on one area of the wall, rather than distribute throughout the whole surface.

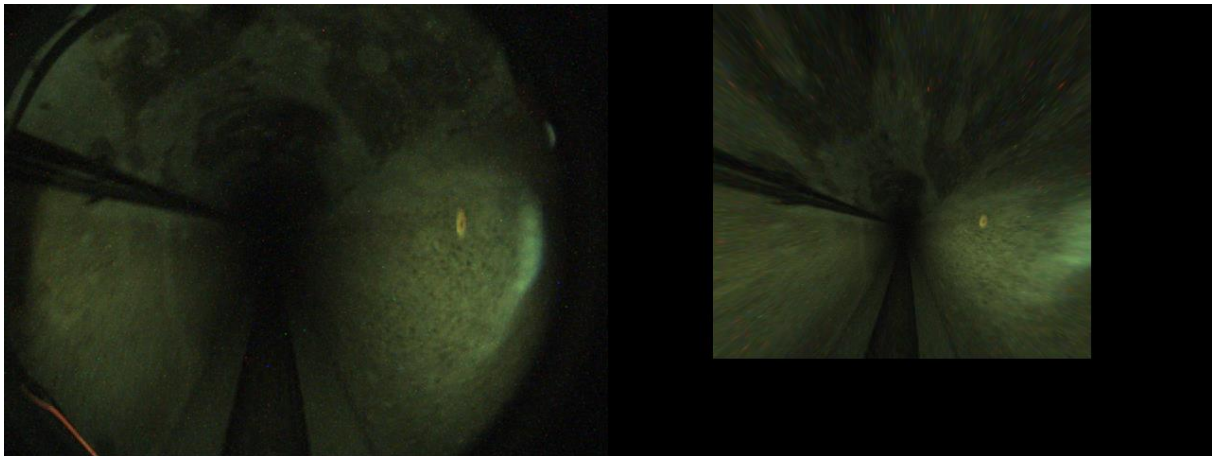


Figure 8 Image taken by the camera in the front of the platform (left) and its rectification (right)

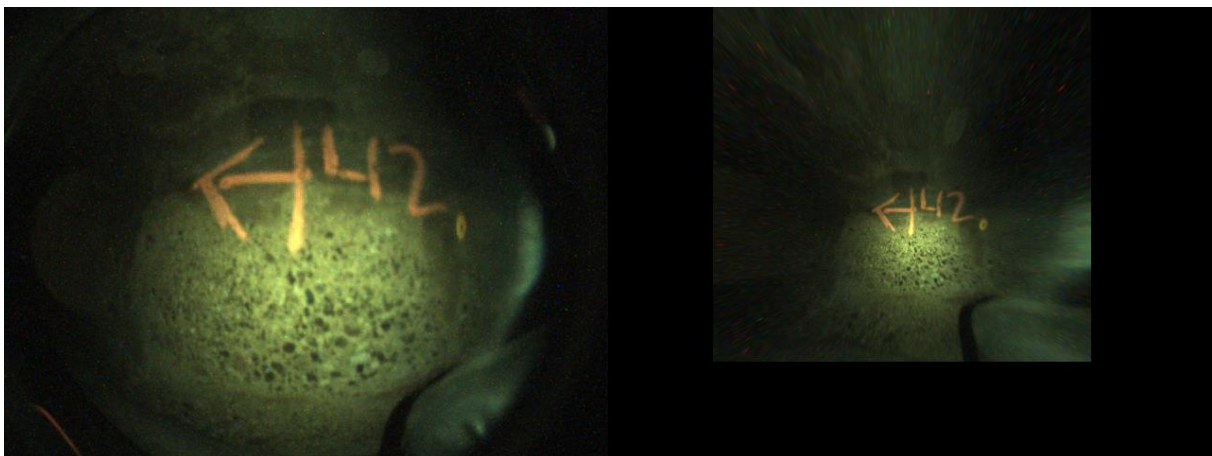


Figure 9 Image taken by the camera on the side of the platform (left) and its rectification (right)

### 3.4.2 Second test - 2016/03/10

In the second experiment the ueye camera was tested. Additionally, a new configuration of the VOLO LEDs (2 units per camera in a distributed configuration) was tried out. The ueye camera passed successfully the test, but we observed that the illumination system needed yet another iteration. Whereas the LEDs on the sides and top of the platform were providing good contrast and definition on the walls, given their proximity to the platform, the LEDs placed in the front of the platform were not capable of casting light enough for the camera to see the scene, since they were facing the darkness of the sewer.

### 3.4.3 Third test - 2016/05/19

This experiment was primarily focused on illumination. The [CREE LEDS model 941-XHP70A10D0HM245G](#) were tested on the front of the platform. The choice of this type of LEDs was satisfactory, but the colour temperature was too low (4500°K) and this would affect the histogram of the images. CREE Leds with high colour temperature were purchased.

### 3.4.4 Fourth test - 2016/06/09

In the last experiment the [CREE LEDS model 941-XHP70A01DOBN20E1](#), with colour temperature 6200°K, were tested, along with the configuration of the cameras and VOLO LEDs on the last designed of the platform. In this experiment the optimal intensity for the CREE LEDs was iteratively selected. The selection of the intensity taken by the CREE LEDS was done by taking videos at different intensities. We also took into account the behaviour of the LEDS, by which their light efficiency increases with time. A trade-off between power efficiency and image definition was found. The overall results were highly satisfactory, with optimal image quality and lighting conditions. Video data was collected, but unfortunately due to technical problems we cannot show them in this document. This video will be shown nonetheless during the demo that will be displayed during the evaluation test of July.

### 3.4.5 Further design

The quality of the images offered by the BFM1220 lens can be improved to the standards of the image sensor of the ueye camera. For this reason we are at the moment testing another lens, model BF2M15520C, but have not experiments in the sewer with this lens since we have given priority to the flight tests. As mentioned in section 3.1.2, a decision over weight restrictions and image quality is to be taken yet.

In Figure 8 and Figure 9 it can be noticed that the area taken of the lens is only a fraction of the whole section, which means that much useless data is sent when video streaming. Equally this setup data storage would be inefficient. We have decided therefore to re-implement the ROS driver in use (see section 3.3) to add in specific functionalities of the camera. These functionalities allow us to select a specific ROI and to set up image variables that will affect the appearance of the image, such as exposure time, gain, dark level, gamma, pixelclock. We need to be able to tinker with these variables to optimize the imagery taken with the low lighting conditions of the sewer. As mentioned in the section 3.3, this driver is able to trigger images on the camera at different frame rate to the frame rate at which images are streamed or saved in memory. This feature allows us to avoid blurring effect as we minimize the amount of data transferred either to the computer or to the base station. As with the lens BFM15520C, this new driver has not been validated in the sewer yet.

### 4 Communications

In this section we present the results of the various test carried out to develop and validate the communications strategy described in deliverable D2.1.

#### 4.1 Test area

To study wireless propagation inside the sewer system, we have selected the test area, composed by one block located in Passeig Sant Joan in Barcelona (see Figure 10). The block is comprised of four street segments: Passeig Sant Joan, Valencia, Bailén and Mallorca.

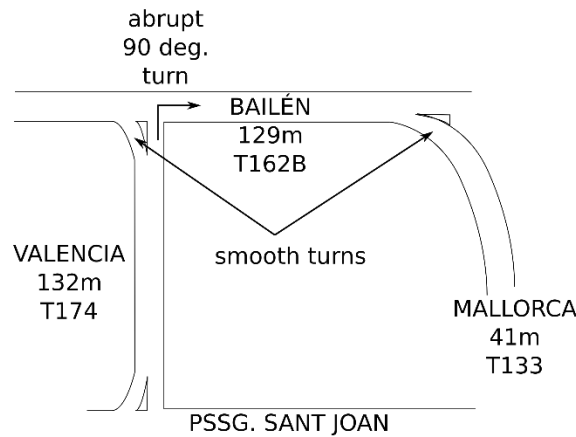
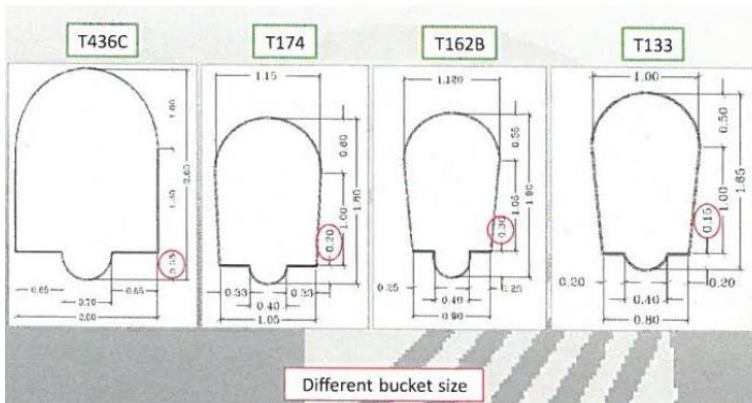


Figure 10 Test area near Passeig Sant Joan in Barcelona

This area exhibits both Line-of-Sight (LoS) and Non Line-of-Sight (N-LoS) conditions, abrupt 90 degrees turns as well as smooth turns. Also, each sewer section has slightly different bucket shape and size.



Different types of buckets (cross-section)



Smooth turn between Valencia and Bailen

Figure 11 Example of sections and turns

## 4.2 Wireless propagation simulations in sewers:

As presented in [8], under certain wireless transmitter-receiver configurations (antenna position and orientation), a periodic and stationary spatial-fading pattern can be obtained inside a tunnel, which can be helpful to characterize propagation (e.g. determine the attenuation rate), and even for localization purposes [9][10].

The analysis of the propagation of electromagnetic waves inside tunnels with arbitrary cross-sections is not analytically feasible. Even for simple geometries, such as rectangular or circular cross sections, no exact closed form solutions are available [5]. Nevertheless, as presented in Chapter 3.5 of [11], for tunnels with uniform cross-section, the Finite Element Method (FEM) calculation of the modal propagation constants and field distribution inside the tunnel is a 2D problem, which can be used to determine the attenuation rate in a straight tunnel segment.

Following that procedure, we used the real profile of the sewer tunnels and solved the attenuation and propagation constants using commercial FEM software, specifically COMSOL [2], in order to determine the attenuation rate inside the sewer as well as the period of the fading structure.

Figure 12 shows the field distribution of the first propagation mode along the cross-section, as well as the received signal strength along a 300m straight tunnel using the real cross-section. These simulations show that at 2.4 GHz, the attenuation rate is about 6 dB/100m. On the other hand, in free space, the attenuation rate is given by the following formula:

$$Path\ Loss(dB) = 32.44 + 20 \times \log(f) + 20 \times \log(D) - G_{tx} - G_{rx}$$

Where:

- $f$  is the operating frequency in MHz,
- $D$  is the distance in km,
- $G_{tx}$  is the transmitter gain in dBi (decibels relative to isotropic)
- $G_{rx}$  is the receiver gain in dBi.

This gives us an attenuation of about 75 dB in 100m in free space using the same setup, compared to the 6 dB in 100m inside the sewer. This makes us believe that, at least in simulations, sewers, as tunnels, behave as waveguides.

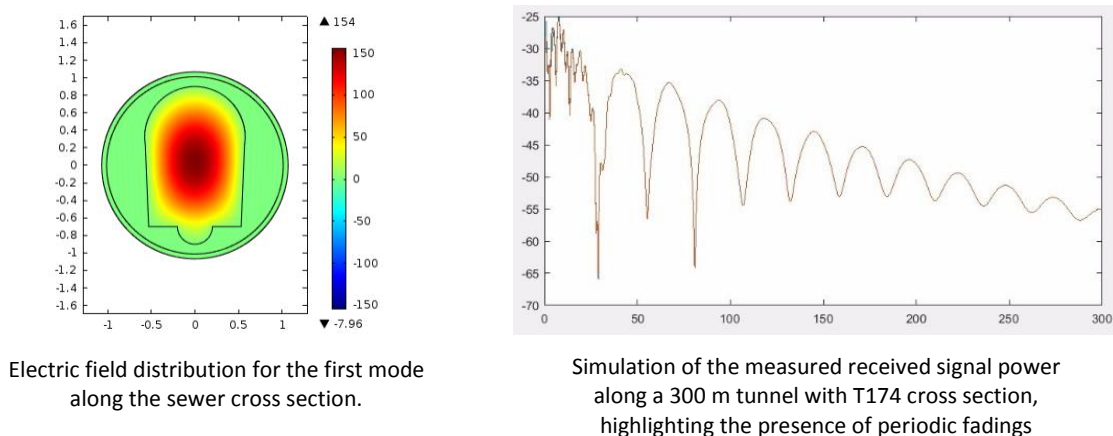


Figure 12 Simulation of wireless propagation in the sewer, using the real cross-section

### 4.2.1 Wireless propagation measuring campaign

To characterize propagation, two computers with an external network card were used (one as transmitter and one as receiver). The network cards have a sensitivity of -95 dBm, and are equipped with Ralink RT2770F chipset. A ROS node was developed to measure the RSS (Received Signal Strength) between the transmitter and the receiver.

The transmitter broadcast frames at a configurable rate, and the receiver node communicates with the network card driver to obtain the measured RSSI (Received Signal Strength Indicator). The tests were conducted at 2.4 GHz, with the transmitter broadcasting frames every 5 ms at a power of 20 dBm. All antennas used were dipoles, with a 2.15 dBi gain. The transmitter was placed at different points according to the test, and will be specified in each case.

#### 4.2.1.1 Valencia: straight segment + 90 degree abrupt turn

In the first test, the goal was to analyze propagation along Valencia street. To do so, the transmitter was placed at point A, and the receiver was displaced by a human operator from point A to point B, along 132 meters from the transmitter, logging the RSSI (Figure 13). An approximate constant speed was maintained along the whole segment, allowing to derive the position estimation at a certain moment.

Results are shown in Figure 14, where we can appreciate spatial fadings with a period of about 25 m, and an attenuation of about 8 dB in 100m.

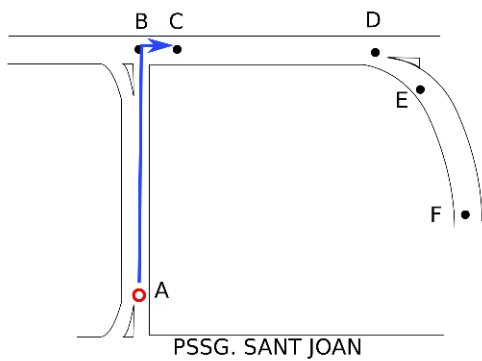


Figure 13 Travelled path in communication along Valencia

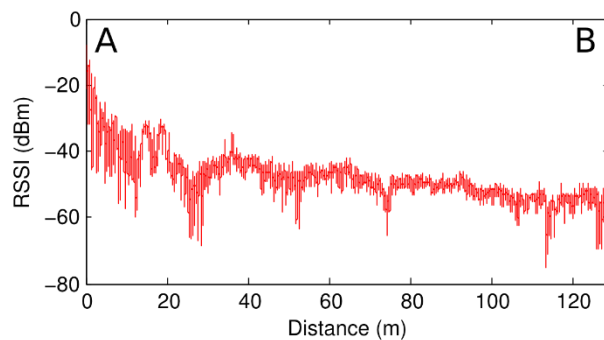


Figure 14 Measured received signal power along Valencia

With these results, we have corroborated both the waveguide behavior, which allow to greatly extend the coverage in comparison to free space, and the fading phenomena.

#### 4.2.1.2 90 degree abrupt turn

Following the previous test, the receiver was moved from point B to point C, while the transmitter was kept at point A. In this condition, we have N-LoS between the transmitter and receiver. As soon as the receiver loses the LoS with the transmitter, the connectivity is lost (in less than 3 meters). No results are shown, due to the fact that if a frame is not received, the RSSI cannot be determined (i.e. non-existence of RSSI=0).

#### 4.2.1.3 Bailén-Mallorca: straight segment + smooth turn

To analyze the influence of the soft turn, the transmitter was moved to point B and the receiver was displaced from point B to point F, passing through point E (Figure 15). Results are

shown in Figure 16. From point B to point D, we can appreciate a similar behavior as in Valencia street: well defined periodic fadings with a mean period of about 22 m, and an attenuation of about 9 dB/100m. The differences with respect to Valencia street are due to the fact that the cross section is slightly different. Later on, at point E (where the LoS with the transmitter is lost), it can be seen that the signal suffers great attenuation. Nevertheless, the received signal still remains above the sensitivity of the receiver. This means that the smooth turn guides the wave softly, making it able to provide communication coverage in a perpendicular street.

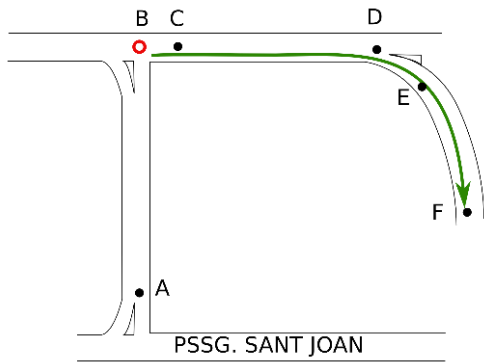


Figure 15 Traveled path in communication along Bailén and Mallorca

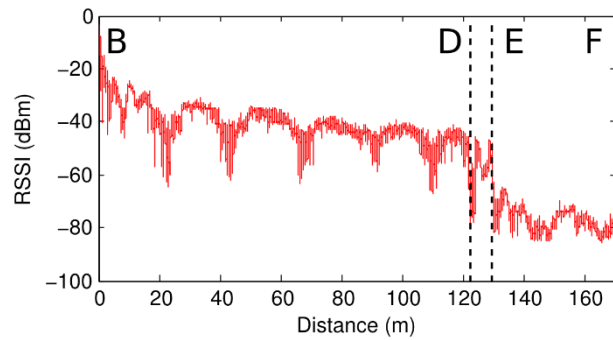


Figure 16 Measured received signal power along Bailén and Mallorca

Table 3 collects the results from both simulations and the measuring campaign. Regarding the attenuation rate, it can be seen that in the real case the attenuation is higher than in simulations. This is caused by the roughness and irregularities along the sewer. Nevertheless, the attenuation is much lower compared to free space, and hence the sewer is acting as a waveguide. With respect to the fadings period, the simulation and the experimental results match quite well.

Table 3: Simulation and Experimental propagation results

Location	Section type	Path Loss Simulation (dB/100m)	Path Loss Measured (dB/100m)	Period Simulation (m)	Period Measured (m)
Valencia	T174	6.06	8	26	25
Bailén	T162B	6.36	9	24	22

Based on the tests performed, we can summarize that:

- Similarly to studies of propagation in tunnels, sewers behave as waveguides: the communication range is extended in comparison to free space, but the signal suffers from fading phenomena. Under certain configurations, these fadings are strictly periodic and can be used for localization.
- In the abrupt 90 degree turns, the signal is lost almost as soon as the LoS between the transmitter and receiver is lost, making it impossible to maintain communication along perpendicular streets.
- The smooth turns attenuate the signals, but also guides it, making it possible to provide coverage along perpendicular streets.

## 4.2.2 Wireless network full coverage test

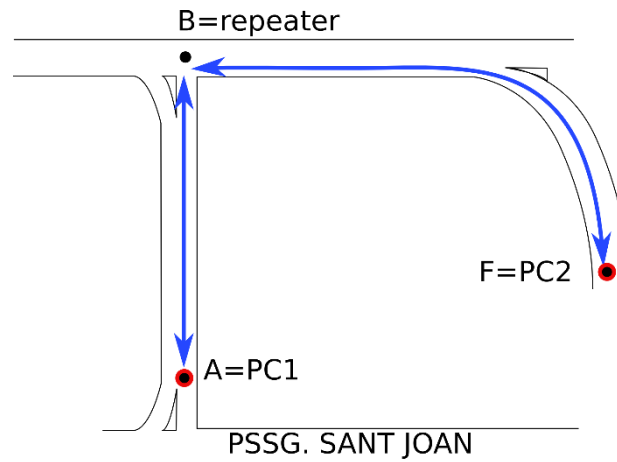


Figure 17 Network deployment to provide coverage along Valencia, Bailén and Mallorca

Considering the previous results, a communication design test was performed in order to provide coverage along Valencia, Bailén and Mallorca. To do so, a repeater was placed at point B, to be able to make an abrupt 90 degree turn. Then, the signal would travel being guided by the soft turn, up to Mallorca.

A computer was placed in point A, a repeater was placed at point B, and a second computer was placed at point F (Figure 17). Ping and text streaming was successfully achieved between both extremes. To make a more detailed study about the available bandwidth at these points, a bandwidth measuring campaign was performed on a different day.

## 4.3 Bandwidth measurement results

Following the wireless propagation characterization, an extensive measurement campaign was performed to determine the bandwidth of the link between the robot (drone) and the base station (BS), specifically in eight strategic points (A to I in Figure 19), under LoS and N-LoS conditions, with and without the use of a network repeater to overcome the problems related to the turns, described in the previous section. Two frequencies were tested: 2.4 GHz and 5.2 GHz.

To measure the bandwidth, the JPERF [3] software was used, which generates traffic to measure the capacity of the link by estimating the time required to send and receive large amounts of data. In each of the points, a sequential bi-directional link bandwidth measurement was performed. The drone was left static for a period of 120 seconds. In the first 60 seconds, the bandwidth of the BS-drone link was measured, followed by the drone-BS link. The base station was kept fixed at point A, and the repeater at point C. The robot was moved from point B through I. Figure 18 shows a screen capture of the bidirectional bandwidth test using the JPERF software.

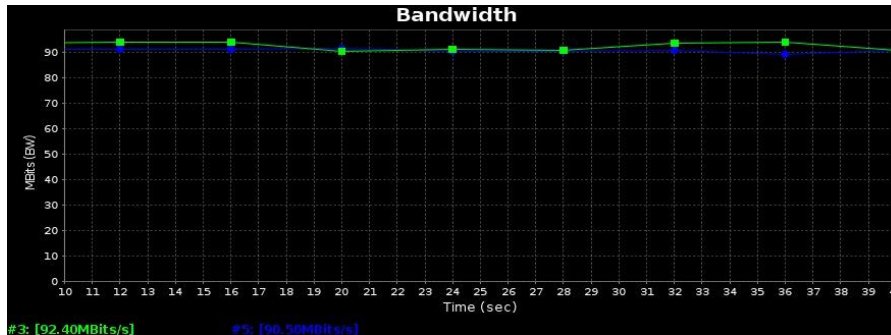
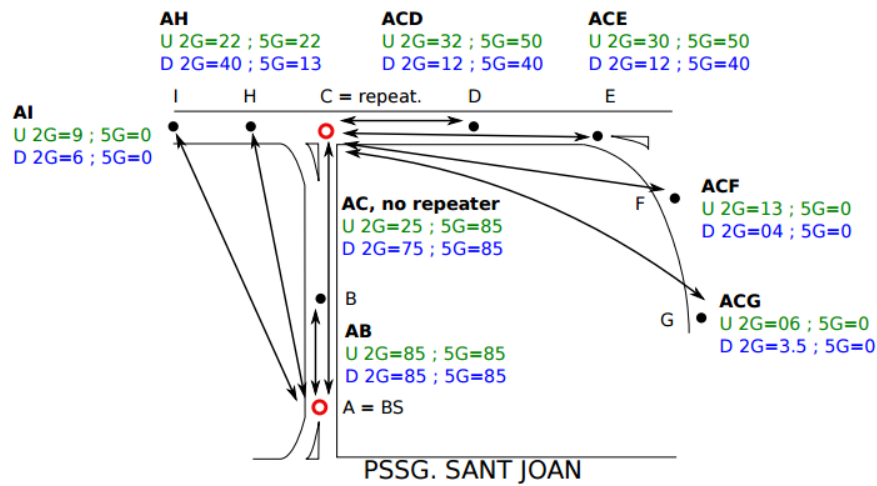


Figure 18: Bandwidth link test example using JPERF

Results are showed in Figure 19. The letter U represents the BS-drone link, while letter D represents the contrary. 2G and 5G represent the frequency, 2.4 and 5.2 GHz respectively. Finally, the units are represented in Mbps. As an example, U 2G=85 means BS-robot link, at 2.4 GHz, and the obtained mean bandwidth was 85 Mbps. Finally, the bold letters represent the path (eg. AH is the link between points A and H without using the repeater, while ACG is the link between A and G, passing through the repeater located at C).

After the tests performed, we can summarize that:

- Under LoS conditions, the bandwidth is higher at 5.2 GHz compared to 2.4 GHz.
- As in the previous section, the signal is not able to make the abrupt 90 turn (point C + 3 m towards point D in Figure 13), at 2.4 GHz nor at 5.2 GHz.
- At 2.4 GHz, the smooth curved structure is able to guide the signal to the perpendicular street (point A to point H and I, or point C to point F and G). At 5.2 GHz, the signal is not guided by the smooth turn. This can be explained by the fact that the wavelength of the signal is much smaller and gets affected by surface irregularities and roughness.



**U: BS-drone**  
**D: drone-BS**  
 2G=2.4 GHz  
 5G=5.2 GHz  
 Units in Mbps  
 e.g. U 2G=85 means BS to DRONE at 2.4 GHz, BW=85 Mbps

Figure 19: Bandwidth link test results

#### 4.4 Antenna polarization

A test was performed to evaluate the influence of the antenna polarization.

The transmitter was placed at point A and the receiver at point C. We have tested a transmitter and receiver in horizontal-horizontal orientation, vertical-vertical, and the cross-polarized case, yielding approximate results. This makes us conclude that polarization is not of much relevancy in such short distances inside the sewers.

#### 4.5 Video-streaming

At last, a video streaming test was performed. The compression used was JPEG at 90%, with the camera working at 11.42 Hz, generating a traffic of about 13.8 Mbps.

The test was performed from point A to point I, at 2.4 GHz, to be able to guide the signal with the smooth turn. Until point H, the video streaming is smooth with no interruptions. From point H to point I, some interruptions can be observed (which matches the bandwidth results, as the video streaming was using more bandwidth than the one available).

This issue can be resolved by optimizing video quality, rate and compression settings.

## 5 Autonomous flight modes

In this section we describe the initial implementation and tests carried out in Phase 1 regarding the ARSI flight modes described in section 3.3.2 – Reactive Navigation of the ARSI design deliverable D2.1.

These semi-autonomous flight modes are designed to help pilots by using live sensor data to automatically correct the vehicle position inside sewer tunnels. Pilots are able to control high-level properties such as inspection speed or heading, while the onboard ARSI software takes responsibility of the lower-level control to keep the vehicle safe in narrow and complex flight environment.

### 5.1 Software design and implementation

The ARSI platform uses a [3DR Pixhawk](#) autopilot system with the [PX4](#) firmware. Pixhawk uses the Micro Air Vehicle Communication Protocol ([Mavlink](#)) to broadcast information from its internal sensors (accelerometers, barometers, compass, etc.), its health status (state, battery life, etc.) and information regarding the Autopilot (control mode, waypoints, etc.). Since all our software system is based on ROS, we use the [Mavros](#) interface to translate all messages between Mavlink and ROS.

The Pixhawk autopilot controller is based on a Cascade Proportional-Integral-Derivative (PID) model, and its architecture allows users to issue control requests at any level of the cascade (position, velocity or attitude requests). This open controller interface allows us to control the ARSI platform by injecting attitude requests into the control loop.

The ARSI platform also carries a Hokuyo 2D laser, which we interface with using the official open-source ROS driver [urg\\_node](#). The driver publishes laser data in the form of standard `sensor_msgs/LaserScan` messages.

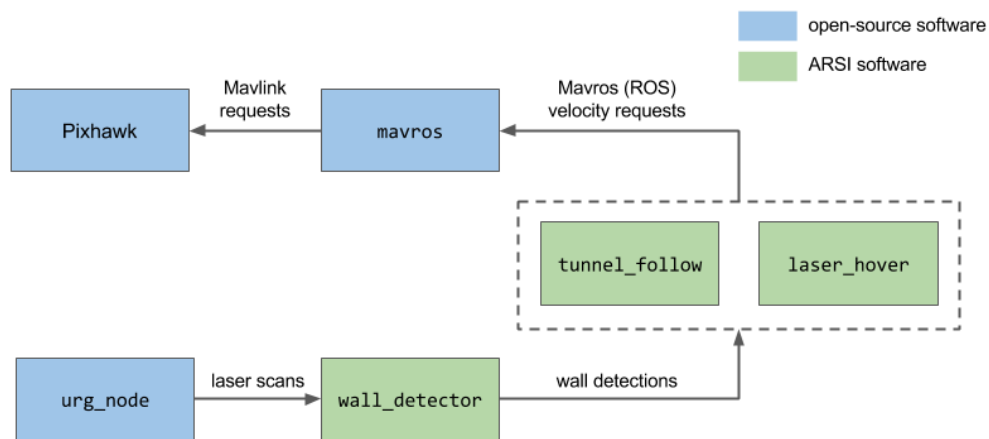


Figure 20: High-level design for the ARSI flight modes

Following the functional design detailed in D2.1, a software design was derived to integrate the ARSI flight modes with the Pixhawk/Mavros architecture, as illustrated in Figure 20. Three separate ROS nodes were developed:

- The `wall_detector` node processes 2D laser data and uses image processing techniques (RANSAC line fitting) to extract information about the geometry of the walls (if any) surrounding the ARSI vehicle during a flight.
- The `tunnel_follow` node implements the “Tunnel Flight Mode” described in D2.1. It uses information about the geometry of the surrounding walls to estimate the trajectory correction required to position the ARSI vehicle at the centre of the sewer (see Figure 21). Attitude requests are derived from the positional error, and sent to the Pixhawk Autopilot via Mavros as `mavros/setpoint_attitude` messages.
- The `laser_hover` node implements the “Hover Flight Mode” described in D2.1. The node processes incoming LaserScan messages, and uses a scan-matching algorithm [1] to estimate the displacement of the ARSI vehicle from the location where the flight mode was enabled. Attitude requests are derived from this displacement and are sent to the Pixhawk Autopilot in order to maintain the platform in a fixed position (hover).

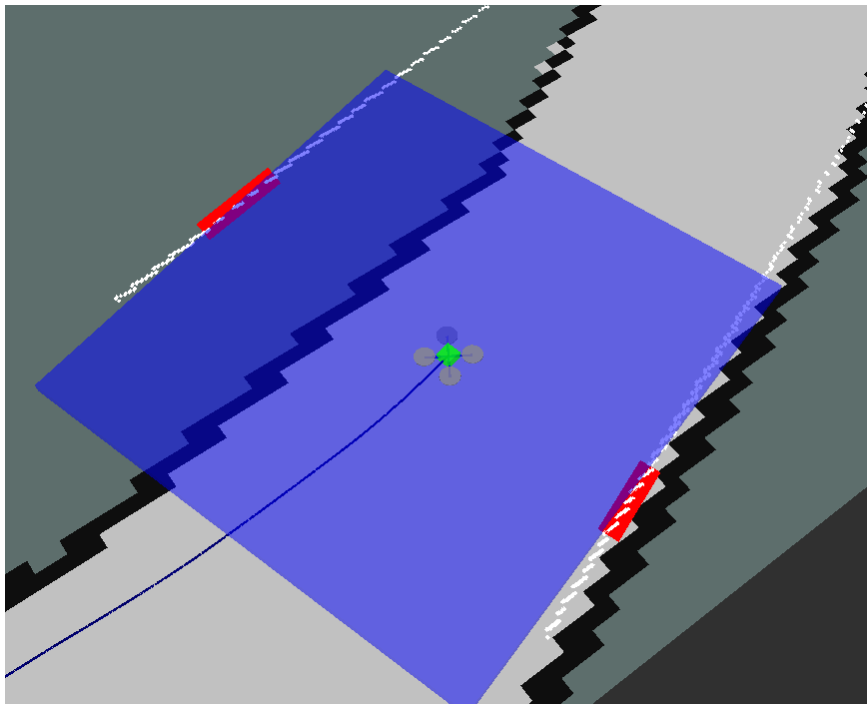


Figure 21: Tunnel mode simulation in RVIZ. Wall detections (in red) are extracted from simulated laser data (in white) to produce tunnel estimations (in blue) used to calculate control requests allowing the vehicle to autonomously follow the tunnel.

## 5.2 Test setup

The software system described above was tested in a simulation environment.

### 5.2.1 Simulator

We used the [JMavSim](#) simulator in a “Software In The Loop” (SITL) configuration, so that both the PX4 autopilot and the ARSI onboard software could run in the exact way that they would in real operations. JMavSim simulates the vehicle physics and dynamics, and we developed a simple 2D laser simulator node (`Laser_sim`) to generate laser scans based on custom-made 2D maps designed to resemble a sewer network.

### 5.2.2 Remote control

In order to replicate the ARSI Concept of Operations described in D2.1, we integrated a USB remote control in our system.

First, we contributed to the `mavteleop` open-source node in the `mavros_extras` ROS package, to allow us to set up a configurable interface between `mavros` and different types of USB remote control (flight controllers, gamepads, etc.). Using this node, we were able to fly the simulated vehicle in all [PX4 flight modes](#): Manual, Altitude Control, etc.

Then we needed to be able to switch between standard PX4 flight modes and our custom ARSI modes. PX4 implements this functionality with the concept of “offboard” modes, in which the firmware delegates control entirely and simply executes control requests issued by a third-party. We developed a utility node allowing us to start and stop our control nodes (`tunnel_follow` and `laser_hover`) depending on the switches on the Remote Control. With this approach, pilots can seamlessly switch between PX4 or ARSI flight modes using any USB remote control.

### 5.3 Test results

As previously mentioned, the system was tested using custom maps simulating different configurations of sewer tunnels. Our `laser_sim` node used the maps to generate simulated laser data, while `JMavSim` and `mavros` were used to simulate the ARSI platform.

We were able to arm the vehicle and take-off in Manual mode using the USB controller, then switch to “Tunnel Follow” flight mode and start autonomously following a sewer. From there we were able to consistently track the tunnels, even with moderate random noise added to the laser data and along moderate bends (see Figure 22).

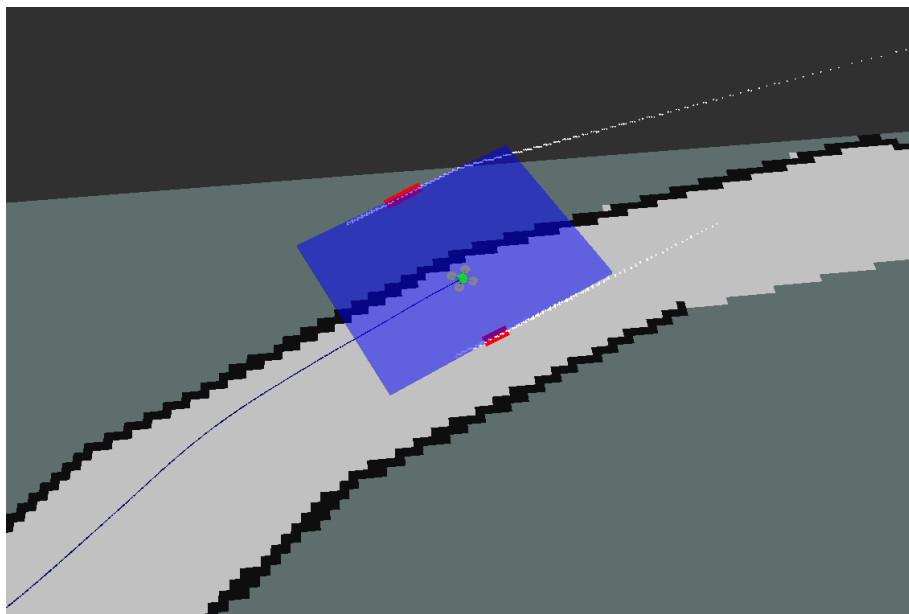


Figure 22: Our tunnel Follow flight mode keeps the vehicle at the centre of the tunnel without human interaction

When reaching a bifurcation, we could switch to “Laser Hover” mode from the remote and engage the scan matcher to hold position accurately and using only laser data.

We feel that our test results are encouraging in that they validate our Concept of Operations. Using a simple USB remote, pilots are able to operate the ARSI platform remotely and can switch between both standard and custom flight modes seamlessly. The two flight modes designed for ARSI greatly simplified the task of flying through a network of tunnels.

Our initial tests also highlighted shortcomings in the control of the platform, occasionally resulting in large errors in sharper bends and intersections. This issue will need further investigation in Phase II, using more advanced flight simulators and physics models such as the [Gazebo robot simulator](#) as well as tests with a real platform. Our wall detection algorithm will also require significant improvements in later phases of the project, to improve accuracy and robustness to irregularities in the sewer walls which, we have observed many times during our other tests in real sewers. This is particularly important as the same algorithm will be used for obstacle detection, a critical component of the safety mechanisms of the ARSI system.

## 6 Remote station

In this section we describe the initial work carried out in the development of the ARSI Remote Station described in section 3.4 of the ARSI design deliverable D2.1. While only limited development was carried out in this initial phase of the project, the objective was to demonstrate how the Remote Station will provide intuitive and visual tools to support operators at all stages of the inspection process with the ARSI aerial platform.

### 6.1 Integration with Dracma

Dracma is the cloud-based platform developed by our partners FCC to manage the planning of sewer inspections as well as inspection teams, schedules and reporting. Taking advantage of our partnership with FCC in this project, the ARSI system will be integrated with Dracma both for the planning and data analysis stages.

As described in deliverable D2.1, ARSI provides a plugin for Dracma to support users when planning ARSI missions, so that battery autonomy and Wi-Fi coverage can be modelled and visualized. An early version of this plugin was developed in this phase to validate the concept and design of this integration.

Figure 23 depicts the estimated Wi-Fi coverage from a point selected by the user. Using this display, operators can plan missions by selecting sections to inspect as well as entry/exit points which must all be within battery range as well as Wi-Fi coverage.

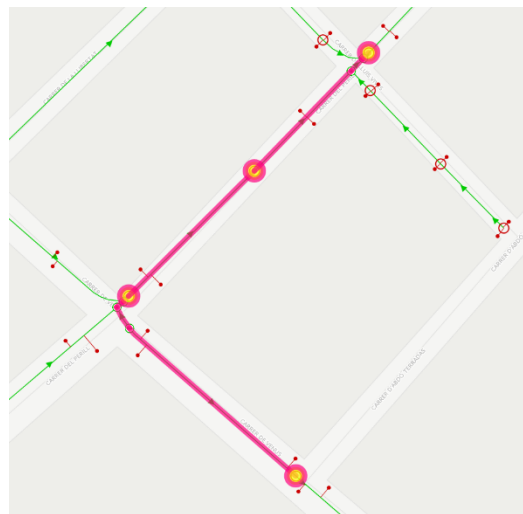


Figure 23: ARSI Wi-Fi coverage displayed in Dracma

### 6.2 Remote station plugins

As described in the ARSI System Design, the Remote Station is designed as a modular platform based on the plugin-based architecture of the open-source ROS tool [RVIZ](#). In order to validate our design, and to provide useful support tools for our various test in the Barcelona sewers, early versions of several plugins were developed in this first phase of the project.

Figure 24 below shows the ARSI Remote Station developed during Phase 1. The main window shows the GIS of the sewer network provided by BCasa overlaid over a satellite map of Barcelona. The left-hand sidebar contains several plugins:

- Vehicle status: displays the contents of various Mavros messages informing users of the state of the vehicle and autopilot;
- Battery status: displays battery voltage, current and remaining time;
- Air monitoring: displays the various levels measured by the Envira air sensor.
- GIS display: allows users to select GIS source from DXF file or PostGIS database, as well which data layers to display.

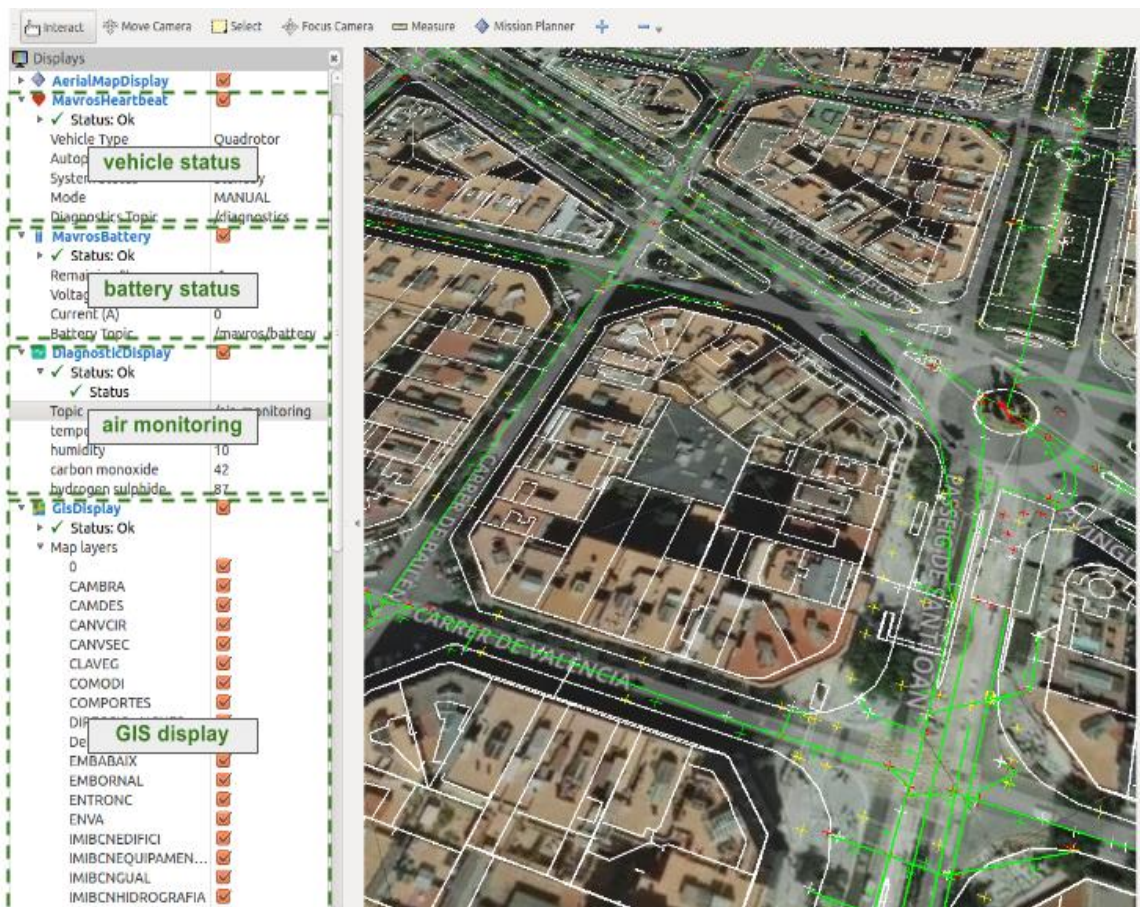


Figure 24: ARSI Remote Station

## 7 Annex A: References

- [1] An ICP variant using a point-to-line metric. In Proceedings of the IEEE International Conference on Robotics and Automation (ICRA). Pasadena, CA, May 2008
- [2] COMSOL. <http://www.comsol.com/>
- [3] <https://iperf.fr/>
- [4] D.G. Dudley, M. Lienard, S.F. Mahmoud & P. Degauque. Wireless propagation in tunnels. Antennas and Propagation Magazine, IEEE, vol. 49, no. 2, pages 11–26, april 2007.
- [5] A. Emslie, R. Lagace & P. Strong. Theory of the propagation of UHF radio waves in coal mine tunnels. Antennas and Propagation, IEEE Transactions on, vol. 23, no. 2, pages 192–205, Mar 1975.
- [6] J.M. Molina-Garcia-Pardo, M. Lienard, A. Nasr & P. Degauque. On the Possibility of Interpreting Field Variations and Polarization in Arched Tunnels Using a Model for Propagation in Rectangular or Circular Tunnels. Antennas and Propagation, IEEE Transactions on, vol. 56, no. 4, pages 1206–1211, April 2008.
- [7] Carlos Rizzo, Francisco Lera & Jose Luis Villarroel. Transversal fading analysis in straight tunnels at 2.4 GHz. In ITS Telecommunications (ITST), 2013 13th International Conference on, pages 313–318, Nov 2013.
- [8] Carlos Rizzo, Francisco Lera & Jose Luis Villarroel. UHF and SHF Fading Analysis Using Wavelets in Tunnel Environments. In Vehicular Technology Conference (VTC Fall), 2013 IEEE 78th, pages 1–6, Sep 2013.
- [9] C. Rizzo, V. Kumar, F. Lera & J. Villarroel. RF Odometry for Localization in Pipes Based on Periodic Signal Fadings. In Intelligent Robots and Systems (IROS), 2014 IEEE/RSJ International Conference on, Sep 2014.
- [10] C. Rizzo, F. Lera & J.L. Villarroel. A Methodology for Localization in Tunnels Based on Periodic RF Signal Fadings. In Military Communications Conference (MILCOM), 2014 IEEE, pages 317–324, Oct 2014.
- [11] Carlos Rizzo. Propagation, Localization and Navigation in Tunnel-like Environments. PhD Thesis. Universidad de Zaragoza, Jul. 2015. Available online: <http://zaguan.unizar.es/record/31897/files/TESIS-2015-080.pdf>